

Fringing in the WFC3/UVIS detector

Michael H. Wong

Astronomy Department, University of California, Berkeley CA 94720-3411

Abstract. In late 2010, a star cluster will be observed with narrowband red filters to determine the impact of fringing (position- and wavelength-dependent patterns of brightness variation) on flight data. Ground flat fields show peak-to-trough amplitude variations of 0.5% to 16% (among 12 affected filters). Different “fringe flat fields” created by models will be applied to the flight data to compare corrections. Two separate sets of ground test data provide different thickness maps (and thus create different fringe flats). The disagreement between the thickness maps is consistent with an error in the monochromatic illumination wavelengths in one of the ground test data sets, but an unexplained corner-to-corner slope across the detector remains even after correcting for the wavelength error. Flight data are needed to determine which thickness map produces the best correction for fringing, and improvements to fringe data analysis may be needed to improve the correction.

1. Introduction

Fringing is caused when multiple internal reflections within a detector lead to constructive and destructive interference. “Wood grain” patterns appear because the phase of the interference is strongly sensitive to detector thickness and wavelength of illumination. In WFC3’s UVIS channel, fringing is detectable only at long wavelengths, where silicon grows transparent enough that some incident photons can reflect off detector layer interfaces, before these photons are absorbed. Fringing is a common issue with astronomical CCD detectors such as WFC3/UVIS, in which the silicon substrates are thinned so that photoelectrons are generated close to the gate structures. Thinning improves detection efficiency at short wavelengths, but leads to more severe fringing effects at longer wavelengths.

In Section 2 I use long-wavelength narrowband UVIS flat fields to estimate the impact of fringing. Section 3 discusses two separate ground test data sets, obtained by illuminating the UVIS detectors with monochromatic light sources. These two data sets are being used to characterize the detector. These data are crucial inputs to models (Section 4) of the UVIS fringing effect. These models produce maps of the detector’s thickness across the entire CCD (Section 5). Reconciling the two ground test data sets has been hampered by an apparent error in the wavelength calibration of one of the data sets (Section 6). On orbit data are now being collected to compare fringe model solutions, and additional tricks may be required to achieve the best correction (Section 7).

2. Estimated Impact of Fringing

Figure 1 shows the effect of fringing by comparing flat fields for two filters in a single quadrant of the UVIS detector: F673N (left), in which fringing is not apparent, and F906N (right), which shows strong fringing effects due to the filter’s slightly narrower bandpass and much longer central wavelength.

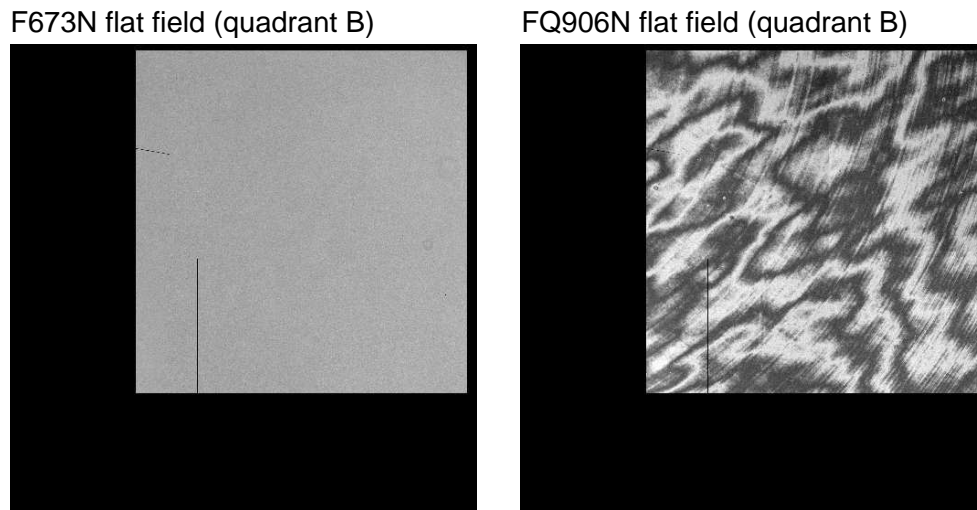


Figure 1: Quadrant B of two ground flat fields: affected by fringing (right) and not affected (left). Black region of the FQ906N flat is masked to avoid areas affected by the quad filter edges; the same region of F673N is masked for consistency. Image scale runs from 0.85 (black) to 1.10 (white), with a square root stretch to emphasize low-level detail.

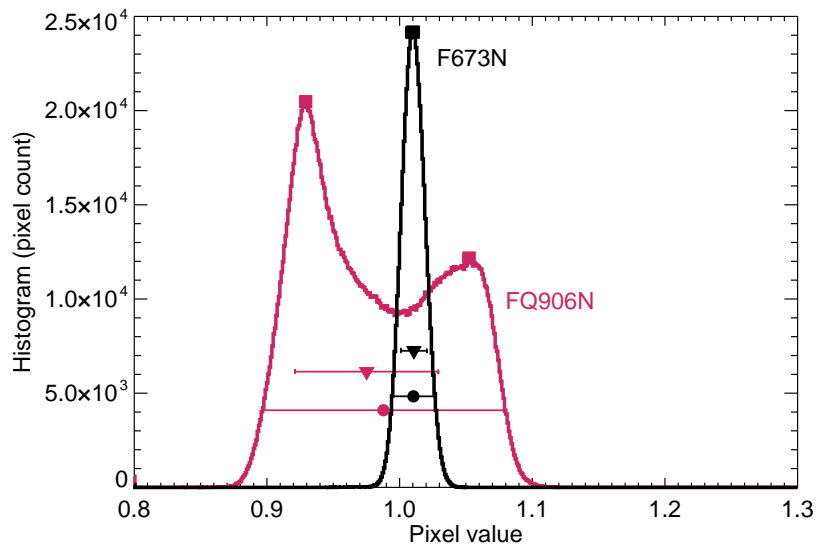


Figure 2: Histograms of the two flat field samples shown in Figure 1. Symbols correspond to fringe amplitude metrics listed in Table 1: rms deviation (triangles with error bars), full width at 20% maximum (circles with error bars), and bimodal histogram peaks (squares).

Analysis of these flat fields provides a generic estimate of the effect of fringing on observations using the narrowband red filters. This approach relies on characterizing histograms of pixel values. Four different metrics are listed in Table 1 and graphically presented in Figure 2. The root-mean-square deviation from the mean (triangles in Figure 2) and the full width at 20% maximum (circles) are the most general metrics. The rms deviation may be most useful in estimating photometric uncertainties due to fringing in on-orbit data, while the full width at 20% maximum may be more useful for exposure time calculations. In filters where fringing is very strong, two additional metrics are presented. The distance between bimodal histogram peaks (squares) may also be useful for exposure time calculations, while the manually measured variation in adjacent fringes on the detector (last column of Table 1) gives a sense of the maximum error that may be introduced by dithers of the same scale as the fringe patterns themselves. Values for a single type of fringing metric can be compared to assess the relative impact of fringing on the filters and quadrants listed. An entry for F606W is also listed as a reference case that is not affected by fringing.

Table 1: Estimates of fringing effects on WFC3/UVIS data, based on analysis of ground flat field data (adapted from Wong, 2010b).

Filter	Quadrant	rms deviation (percent)	Full width at 20% maximum (percent)	Distance between histogram peaks (percent)	Manual peak-to-trough (percent)
F606W	A	0.9	2.9	–	–
F606W	B	1.0	3.0	–	–
F606W	C	1.2	3.3	–	–
F606W	D	1.2	3.3	–	–
F656N	A	1.4	4.9	–	2.2 ± 1.2
F656N	B	1.3	4.5	–	1.7 ± 1.1
F656N	C	1.6	5.1	–	1.7 ± 1.2
F656N	D	1.5	5.1	–	3.2 ± 1.3
F658N	A	1.3	4.4	–	–
F658N	B	1.2	3.9	–	–
F658N	C	1.4	4.4	–	–
F658N	D	1.3	3.7	–	0.9 ± 1.1
F673N	A	0.9	3.1	–	–
F673N	B	1.0	3.2	–	–
F673N	C	1.3	3.6	–	–
F673N	D	1.4	4.2	–	0.5 ± 1.1
FQ674N	B	2.1	7.4	–	2.4 ± 1.3
FQ672N	D	2.0	7.0	–	4.6 ± 1.3
FQ750N	B	1.3	4.5	–	1.2 ± 1.1
FQ727N	D	1.6	5.3	–	2.3 ± 1.1
FQ889N	A	3.8	13.5	7.8	10.0 ± 1.3
FQ906N	B	5.4	18.2	12.5	12.2 ± 1.4
FQ924N	C	4.4	16.5	6.9	10.1 ± 1.4
FQ937N	D	5.0	18.4	9.4	14.2 ± 1.4
F953N	A	7.6	23.7	17.8	19.8 ± 1.7
F953N	B	7.8	24.0	17.3	20.8 ± 1.8
F953N	C	7.1	23.5	14.9	17.8 ± 1.7
F953N	D	6.7	22.9	15.0	11.5 ± 1.6

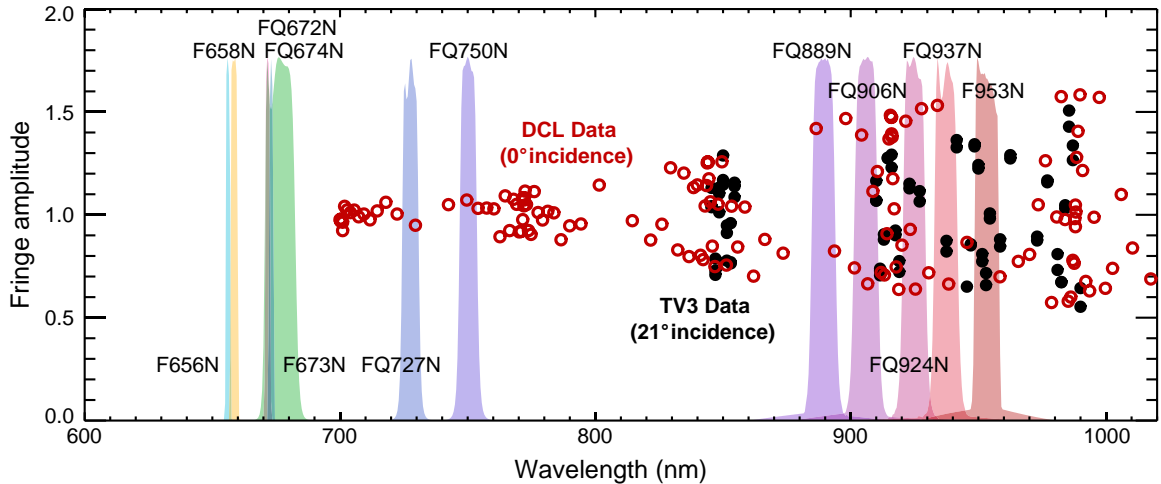


Figure 3: Fringe amplitude as a function of wavelength for DCL (open circles) and TV3 (filled circles) data for a single pixel. Overlaid are normalized bandpasses of WFC3/UVIS narrowband red filters longer than 600 nm, some of which are affected by fringing (see Table 1).

In Wong (2010b) the analysis of flat field data to characterize fringing is described in greater detail, along with images and histograms for every narrowband long-wavelength filter. The flat fields themselves are described in Sabbi et al. (2009).

Science target pixel distributions will differ from those in the flat fields if the spectral energy distribution (SED) of the target differs significantly from that of the calibration light source. Sources with narrow SEDs may be affected by fringing even if they are observed using broad-band filters. Sources with SEDs very similar to the calibration source will have most of the effects of fringing removed by flatfield division (as part of the standard calibration pipeline), but sources with significantly different SEDs may actually have additional error introduced by the pipeline. Section 7 discusses “fringe flats” which can be used to correct for fringing, if the SED of the target is known. Fringe flats can be created based on modeling of extensive sets of ground test data taken for this purpose.

3. The Ground Test Data

Two sets of ground test data were taken to measure fringe patterns as a function of wavelength in the UVIS detectors. The first set of tests were conducted at NASA Goddard Space Flight Center’s Detector Characterization Laboratory (DCL) in 2001. As part of the WFC3 Thermal Vacuum Test 3 (TV3) in 2008, a second set of data were acquired. Differences in experimental conditions between the DCL and TV3 tests are described in greater detail in Wong and Malumuth (2010), and the data are archived as described in Wong (2010a).

Three key differences distinguish the two data sets. The DCL data set contains about twice the number of frames as the TV3 set (~ 150 rather than 77), spanning a wider range of wavelengths. The detectors were illuminated at normal incidence in the DCL configuration, and at a flight-like incidence angle of 21° in the TV3 tests.

Figure 3 compares the ground test data wavelength range with the bandpasses of UVIS’s narrowband long-wavelength filters. Although the TV3 data span the wavelength range that is most strongly affected by fringing (longward of 880 nm; see Table 1), the DCL data have better coverage at the shortest wavelengths. Originally, it was thought that effects of fringing would be limited to wavelengths longer than about 750 nm (Bond and Kim Quijano, 2007). However, ground flats revealed that the cutoff fell closer to 600

nm (Sabbi 2008), with F656N being the shortest-wavelength filter showing visible signs of fringing in flatfield images. The DCL data, due to their better short wavelength coverage, are therefore the most promising test data for use in fringe models (Section 4) used to simulate fringing at short wavelengths.

4. Modeling Fringing

Malumuth et al. (2003a) developed a thin-film analytical model of the STIS CCD to predict and correct fringing effects. The code solves the Fresnel equations, modeling the detector as a series of layers, each characterized by a thickness and a complex index of refraction. The roughness of the interface between each pair of layers is also parameterized. The basic approach is to take a set of calibration data, using the model to find parameter sets that best simulate the data. These parameter sets can then be used to simulate any arbitrary data frame and to correct for fringing. Malumuth et al. (2003b) describes the adaptation of the STIS CCD fringing model to the WFC3/UVIS detector, and the technical details of the parameter fitting approach used in this work is described in Wong (2010a) and Wong and Malumuth (2010). Results of the UVIS modeling effort to date are described in Wong and Malumuth (2010).

Although the CCD assembly is modeled as a system of seven layers (eight including the semi-infinite vacuum above the detector stack) with seven interfaces, the thickness of the silicon detection layer has the greatest effect on fringing. Fits were tested to the TV3 and DCL calibration data for 8000 values of the detection layer thickness, in steps of 0.5 nm. Six sets of secondary parameter values (roughnesses and non-detection layer thicknesses) were also tested. Once the calibration data are used to find best fit model parameters, the parameters can be used to simulate fringing at intermediate wavelengths, or for an arbitrary SED.

Figure 4 compares the two data sets and four model calculations. The model calculations used best-fit parameters for either the DCL or TV3 data sets. The plot shows fringe amplitude as a function of wavelength, for a single representative pixel. Similar results are seen for other pixels. The solid curves indicate that the TV3 (black) and DCL (red) data are well-fit by the models. The DCL data have already been corrected for a wavelength error described in Section 6.

Unfortunately, consistency between the DCL and TV3 data sets has not yet been achieved. The dashed lines in Figure 4 present models based on one set of retrieved parameters (e.g., the dashed red curve is based on TV3 data) but with fringe amplitudes appropriate for the incidence angle of the other data set (e.g., the dashed red curve is model output for 0° incidence as appropriate for comparison with DCL data). The disagreement between the dashed curves and the data points of the same color shows that even with the DCL wavelength correction, the two data sets do not agree. This disagreement is even more severe without the wavelength correction.

5. Thickness Solutions

Detection layer thickness maps are shown in Figures 5 and 6, as retrieved from the TV3 and DCL data sets respectively. Retrievals based on the two data sets result in slightly different thickness maps. Because fringing is so sensitive to detection layer thickness, models using the two thickness maps will predict very different fringing behavior. On-orbit cluster observations are being conducted in filters sensitive to fringing, to determine the best input parameters (thickness map, and secondary parameters map) for the model.

Section 6 describes a correction to the DCL wavelength calibration. With this correction (already applied to the DCL data used to retrieve the Figure 6 thicknesses), the model retrieves similar thickness maps using the TV3 and DCL data sets. Without the

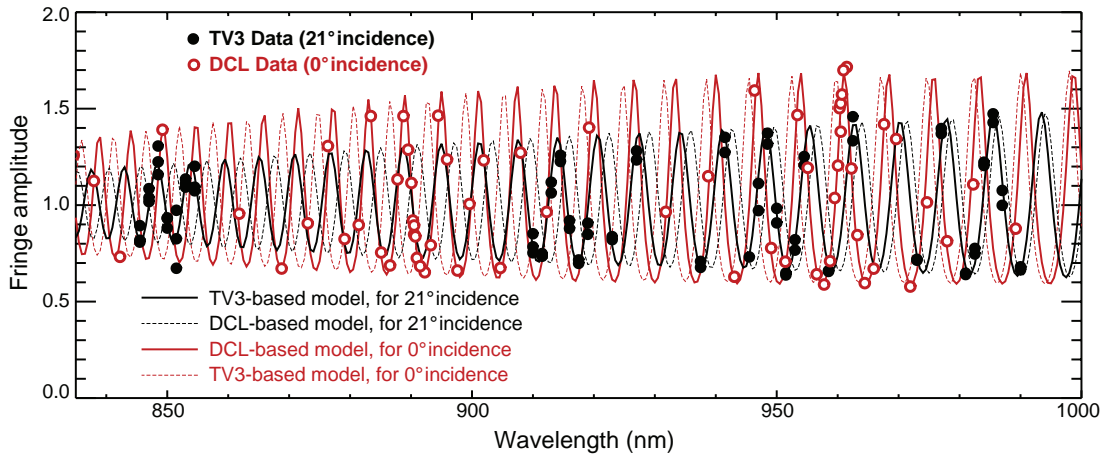


Figure 4: Two sets of fringe data (circles) and four model fringe spectra (curves) for a single Chip 1 pixel at location 1000, 1000. TV3 and DCL data have different amplitude spectra because the incident light angle was different in the DCL and TV3 experiments. Except for a couple outliers near 850 nm, there is excellent agreement between the TV3 data (black circles) and a model fitted to these same data (solid black curve). Likewise, agreement is good between the DCL data (red open circles) and a model fitted to the DCL data (solid red curve). However, there is a problem with combining the two data sets: the dashed lines show that solutions based on one set of data (TV3 or DCL) do not fit the data in the other set. Some DCL data at longer and shorter wavelengths are not shown; all TV3 data for this pixel are shown. The wavelengths of the DCL data have been corrected (see Section 6), and the models were fit to wavelength-corrected DCL data.

wavelength correction, thickness maps derived using DCL data are about $1 \mu\text{m}$ thicker than those derived using TV3 data. Figure 7 shows that the correction improves the agreement so that the retrieved thickness maps differ by less than $0.3 \mu\text{m}$.

Fringe data for a single wavelength is compared to model fringe amplitude in Figure 8. The error bars in the data show frame-to-frame variation among three frames, all illuminated at the same nominal wavelength. The model fringe amplitude data provide an excellent fit within these error bars, but highlight a problem with the fringing solution: that intrinsic noise in the test data limit the accuracy of the retrieved fringe model parameters.

6. The Wavelength Error

Thickness maps retrieved using TV3-only data and DCL-only data differed by about $1 \mu\text{m}$. In Wong and Malumuth (2010), this discrepancy was shown to be partly due to an error in the wavelength calibration of the DCL data. After this correction, the difference between thickness maps based on the two test data sets was reduced to less than $0.3 \mu\text{m}$ (Figure 7).

Measurement of the wavelength error was done in two steps. First, fringe model output for the entire spectral range was calculated using the TV3-derived thickness map. Then, for each monochromatic frame of DCL data, an optimal wavelength was found, such that the residuals were minimized between the test data and the model output. Figure 9 shows this optimal wavelength, plotted as a function of the commanded wavelength in the DCL test data set. A strong systematic relationship is evident.

The ratio of optimal to commanded wavelength is plotted in Figure 10. The mean ratio between 700 and 1000 nm is 0.972 ± 0.003 .

The distribution of data points in the figure is well understood in terms of order errors. Order errors result because fringe amplitude, as a function of either wavelength or

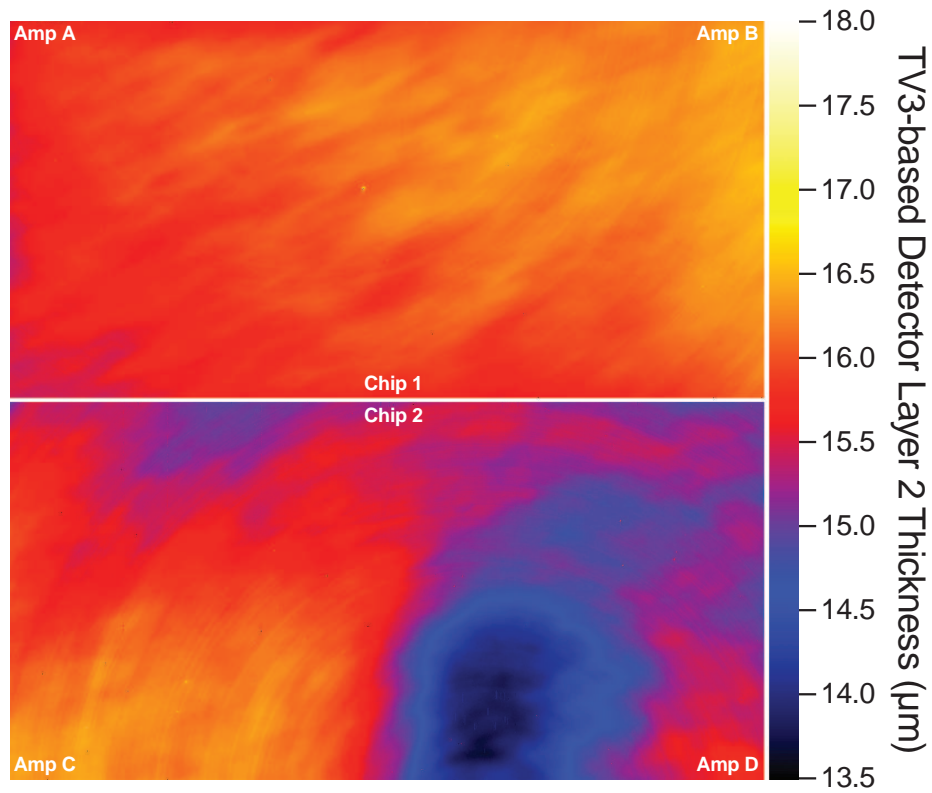


Figure 5: CCD detection layer thickness map based on TV3 data alone. For Chip 1, the median and standard deviation of thickness is $16.04 \mu\text{m} \pm 0.23 \mu\text{m}$, with 1% of pixels thinner than $15.51 \mu\text{m}$ and 1% thicker than $16.46 \mu\text{m}$. For Chip 2, the thickness is $15.42 \mu\text{m} \pm 0.58 \mu\text{m}$, with 1% thinner than $13.87 \mu\text{m}$ and 1% thicker than $16.19 \mu\text{m}$.

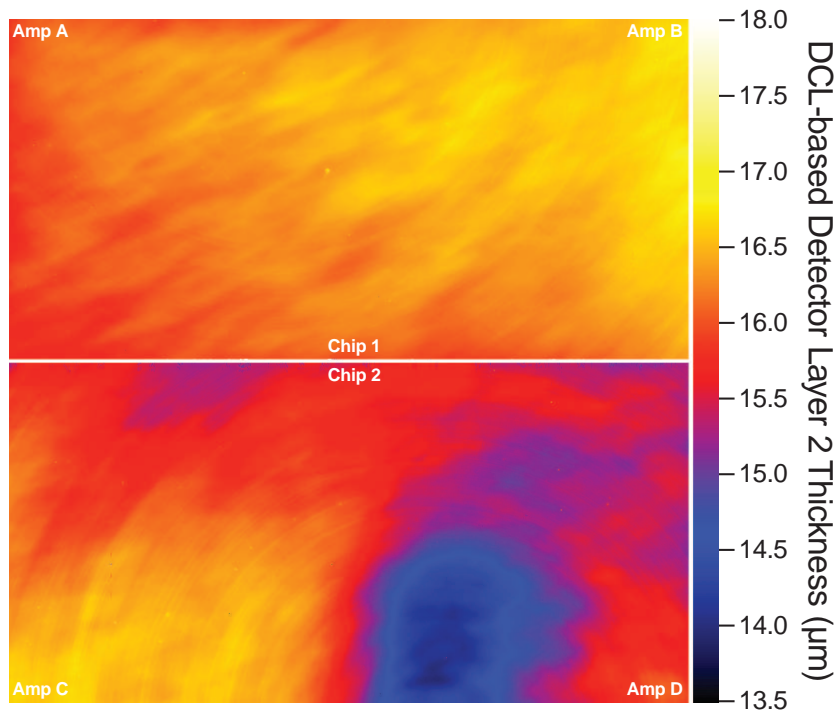


Figure 6: Same as Fig. 5, but for wavelength-corrected DCL data. For Chip 1, the median and standard deviation of thickness is $16.33 \mu\text{m} \pm 0.23 \mu\text{m}$, with 1% of pixels thinner than $15.81 \mu\text{m}$ and 1% thicker than $16.75 \mu\text{m}$. For Chip 2, the thickness is $15.70 \mu\text{m} \pm 0.58 \mu\text{m}$, with 1% thinner than $14.15 \mu\text{m}$ and 1% thicker than $16.64 \mu\text{m}$.

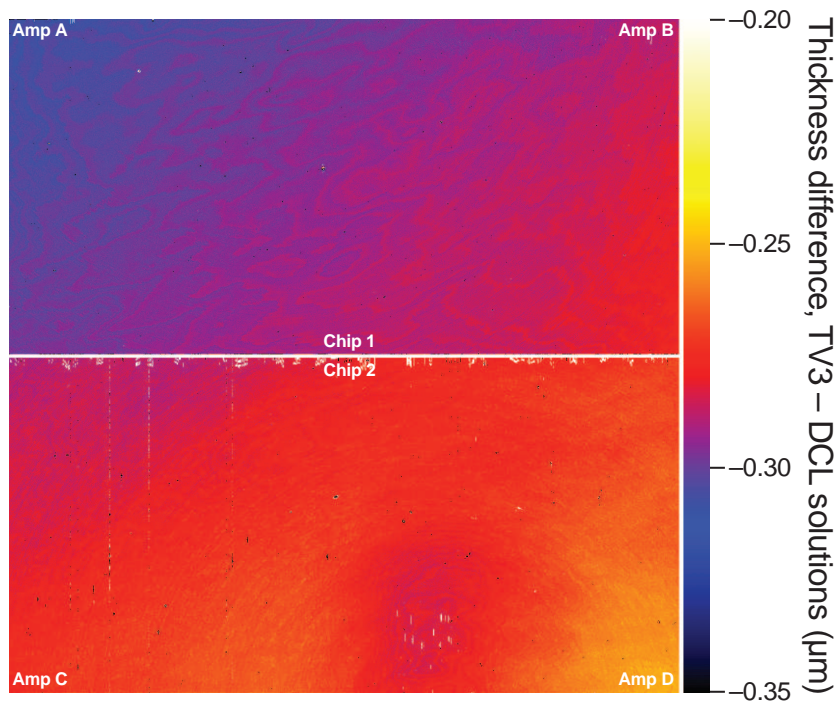


Figure 7: Map of the TV3 thickness (Fig. 6) minus the DCL thickness (Fig. 7). The difference ranges from about $-0.30 \mu\text{m}$ (upper left) to $-0.28 \mu\text{m}$ (lower right) for Chip 1, and from $-0.29 \mu\text{m}$ (upper left) to $-0.25 \mu\text{m}$ (lower right) for Chip 2.

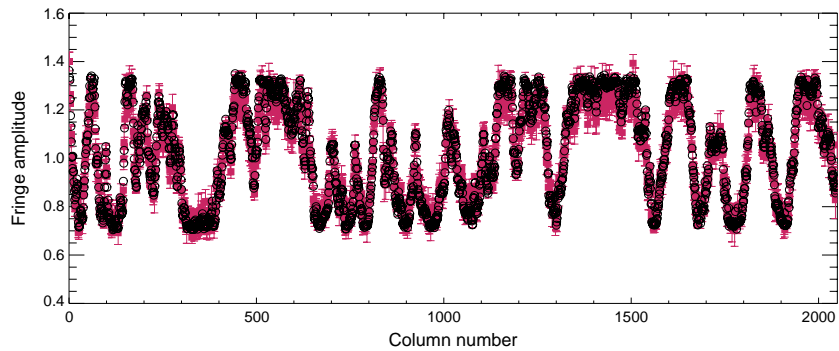


Figure 8: TV3 test data (shaded squares with error bars) and model fringe amplitude (black circles). Data are average values for three frames at 910.00 nm, with error bars showing the standard deviation of normalized signal level among the three frames. Data are shown for column 3000 of Chip 1. Model amplitudes are based on the TV3-derived thickness solution shown in Fig. 5.

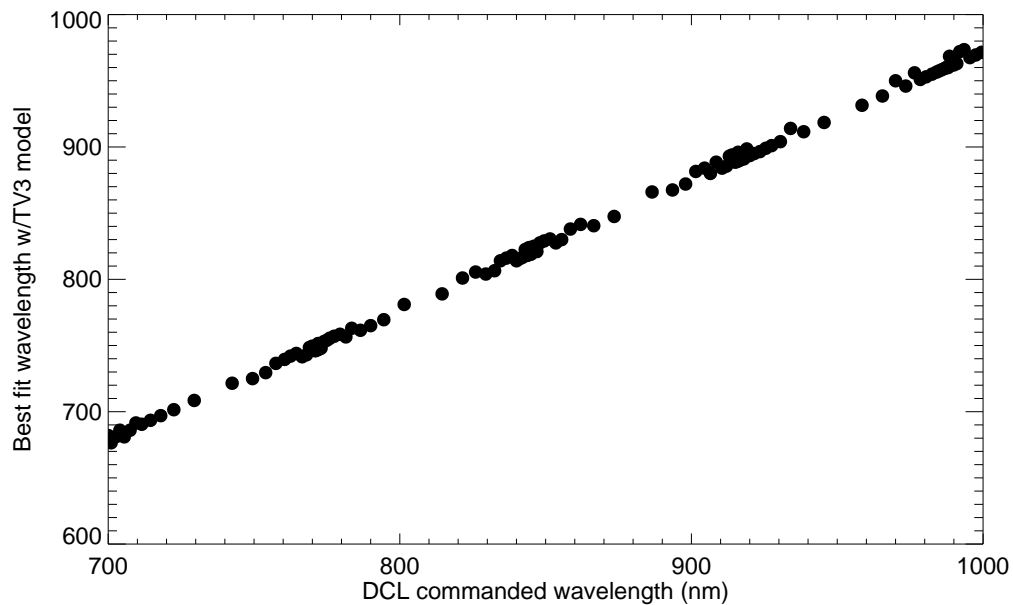


Figure 9: Optimum (y-axis) vs. commanded (x-axis) wavelengths for Chip 2 DCL data frames.

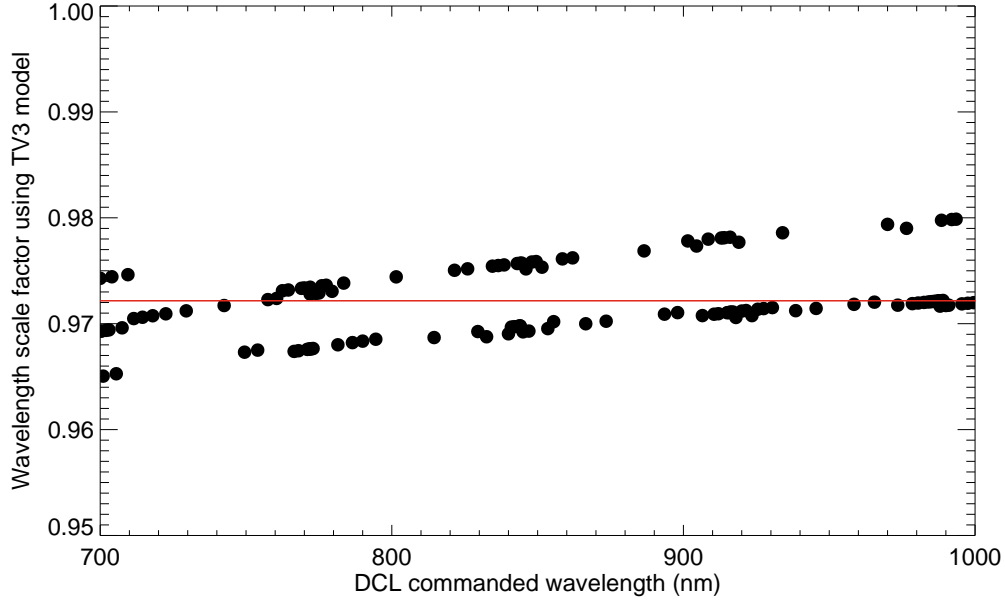


Figure 10: Optimum scale factor vs. commanded wavelength for all the Chip 2 DCL data. Red line shows the mean scale factor of 0.972, with a standard deviation of 0.003.

detection layer thickness, is oscillatory. Fringe amplitude (and thus residuals between data and models) therefore can be very similar for nearby values of wavelength that differ by one order. When adjacent orders of fringing produce very similar residual minima, small amounts of noise in the data can cause automated minimization methods to select one residual minimum over the other in a random fashion. This explains the behavior in Figure 10 near the commanded DCL wavelength of 840 nm, where frame-by-frame values of the optimal/commanded wavelength ratio (black points) are distributed above and below the mean ratio of 0.972 (red line), but do not lie exactly at 0.972. A single wavelength scale factor may be an oversimplification of the problem, because at this wavelength, the optimal wavelength actually corresponds to a local maximum in the fit residuals; two adjacent minima are randomly selected from frame to frame here. Over the entire wavelength range, however, a single wavelength scale factor provides a good fit, because frame-by-frame values oscillate around the mean value of 0.972. Section 7 (and Wong and Malumuth, 2010) discusses possibilities for further refining corrections that may make it possible to combine the two data sets to find a common solution.

7. Future Work

Improvements to the understanding and correction of fringing effects in the WFC3/UVIS detector can be made in four areas: understanding and correcting discrepancies between the TV3 and DCL data sets, using flat field data as input to the fringing model, using on-orbit cluster observations to evaluate various fringe model solutions, and developing fringe-flat software to allow users to correct their data for fringing effects.

Although it is demonstrated above that the wavelength correction to the DCL data considerably improves the agreement between the TV3-derived and DCL-derived thickness maps, three clues show that the correction is not perfect:

- Fringe *amplitude* (at wavelengths shorter than about 850 nm) is better fit by the DCL data without the wavelength correction (Wong and Malumuth 2010).
- The mean difference between retrieved thicknesses is non-zero (Figure 7).
- There is a gradient in the absolute thickness difference map, increasing from lower right to upper left in both chips (Figure 7).

Despite the $\sim 70\%$ better agreement between thickness maps after the wavelength correction, the first clue suggests that no wavelength correction should be applied. It is important to recognize that fringe amplitude is also affected by the secondary parameters (Malumuth et al. 2003b; Wong 2010a). Parameter set maps derived from TV3 data are much closer to uniformly distributed across the six secondary parameter set values, whereas the DCL parameter set maps are dominated by one of the six possible values, again suggesting that the wavelength correction is inconsistent with the fringe amplitudes in the data. The second clue indicates that more work must be done before the two data sets can be combined, but provides little obvious insight.

The third clue makes an interesting parallel with the pattern seen in low-frequency flat field corrections derived from on-orbit data (Sabbi 2010, Rajan 2010), which also show diagonal gradients across both chips. The orientation of Chip 2 was reversed in the DCL tests (Wong and Malumuth 2010), so if the gradient were due to a problem with the DCL data, then it should have a reversed orientation between the two chips. Because the orientation of the gradient is the same in Chip 1 and Chip 2, the problem must lie with the TV3 tests instead. This problem, which may be due to the TV3 illumination source, could have a common origin with the gradient in the low-frequency flat fields. If so, it may be possible to apply the low-frequency flat correction to the TV3 data before solving for detector thickness (and secondary parameters). This approach could provide new results, including an improved wavelength correction for the DCL data.

The entire motivation for including both DCL and TV3 data is to cover a larger wavelength range, and thus to enable fringing correction for shorter-wavelength filters such as F656N. If this is not possible, the TV3 flat field data themselves could be used instead. Monochromatic data are preferable, because they create larger fringe amplitudes (and thus better signal to noise ratios), but a trade for wavelength coverage may make it worthwhile to consider including flat field data as inputs to the fringing model. Again, consideration should be paid to the low-frequency flat field correction identified by Sabbi (2010).

Two Cycle 17 calibration proposals (IDs 11922 and 12091) are being executed to observe the Omega Centauri star cluster in narrow-band red filters affected by fringing. These observations will provide the ultimate test of various fringe corrections, as produced by the Malumuth et al. (2003b) model using parameter sets derived from TV3 and DCL data, or additional parameter sets created after further refinements to the analysis.

Ultimately, the parameter set that best corrects the on-orbit fringe test data will be used to generate fringe flat fields, which can correct science data. Because fringing is a strong function of wavelength, users will need to provide SEDs to the model in order to get fringe flats appropriate for the observations. This includes observations of narrow-band red sources observed through wide filters, because such sources will also be affected by fringing. Modeling fringing in WFC3/UVIS is still at an early stage, with the best correction not yet defined, so work on software to create fringe flats has not yet begun.

8. Conclusions

As measured in ground flat field data, fringing affects narrow-band red filters at the 0.5–16% level. Although pipeline flat fields may correct for most of the photometric error associated with fringing, sources with SEDs significantly different from the calibration source will not

be properly corrected. Two monochromatic data sets (DCL and TV3) were used to retrieve detection layer thicknesses, which can be used to model fringing for any desired SED.

Although thickness solutions for the two data sets disagree, the solutions are more consistent after a correction is made to the wavelength of illumination in the DCL data set by decreasing the wavelength of illumination by a factor of 0.972 with respect to the commanded wavelength. This correction reduces the difference in retrieved detection layer thickness from about 1 μm to about 0.28 μm . However, a gradient in the retrieved thickness difference between the two data sets, diagonally across each chip, implies that further corrections must be made to the TV3 data before retrieving detection layer thickness maps. The gradient resembles the gradient in the low-frequency flat field correction from on-orbit calibration data (Sabbi 2010), and may result from a related cause in the TV3 test configuration. If further analysis is unable to reconcile the two calibration data sets, then it may be useful to include flat field data as a supplementary source of input data to the model, because the TV3 tests did not extend to short enough wavelengths to reliably correct filters at wavelengths less than 850 nm. The use of ground flat data as input data for the fringing model is limited by the degree to which the spectrum of the calibration source is known.

On-orbit cluster observations currently being collected will be the ultimate test of various fringe model parameter sets. Once the optimal parameter set is determined, fringe flats can be generated from the model for any arbitrary SED. Fringe modeling is the only way to correct science data in cases where the SED differs significantly from the calibration source, such as line emission data, or data with strong spectral slopes across filter bandpasses.

Acknowledgments. Thanks to Eliot Malumuth for extensive helpful discussions, for strong collaborative work, and for a ride to the MARC train in his fast car. Thanks also to the staff at GSFC's DCL for their work on characterizing the WFC3 CCDs, the staff at STScI and GSFC who collected the TV3 fringing ground test data (Elizabeth Barker, Howard Bond, Howard Bushouse, Linda Dressel, Bryan Hilbert, Bob Hill, Ray Lucas, Jen Mack, André Martel, S. Rinehart, and last but not least, Megan Sosey), and the entire WFC3 team for their part in making my year as Visiting Scientist one of the most exciting and rewarding experiences in my career. Thanks to Ana-Maria Valenzuela for providing energetic and efficient administrative support, to Elena Sabbi for leading calibration proposal 11922 and providing assistance with calibration proposal 12091, to Larry Petro, whose keen insight and exhaustive knowledge of the WFC3 instrument drove many key brainstorming sessions, and to John MacKenty for his collegiality and leadership at the helm of the WFC3 sailboat.

References

- Bond, H.E., & Kim Quijano, J., ed. 2007, Wide Field Camera 3 Instrument Handbook, Version 1.0 (Baltimore: STScI)
- Malumuth, E.M., Hill, R.J., Gull, T., Woodgate, B.E., Bowers, C.W., Kimble, R.A., Lindler, D., Plait, P., & Blouke, M., 2003a, Publications of the Astronomical Society of the Pacific 115, 218
- Malumuth, E.M., Hill, R.J., Cheng, E.S., Cottingham, D.A., Wen, Y., Johnson, S.D., & Hill, R.S. 2003b, in Future EUV/UV and Visible Space Astrophysics Missions and Instrumentation, ed. J.C. Blades & O.H.W. Siegmund, Proceedings of SPIE 4854
- Rajan, A. ed. 2010, WFC3 Data Handbook, Version 2.0 (Baltimore: STScI)
- Sabbi, E. 2010, CALIBRATION WORKSHOP 2010
- Sabbi, E. 2008, WFC3 ISR 2008-17
- Sabbi, E., Dulude, M., Martel, A.R., Baggett, S., & Bushouse, H. 2009, WFC3 ISR 2008-46
- Wong, M.H. 2010a, WFC3 TIR 2010-01

Wong, M.H. 2010b, WFC3 ISR 2010-04

Wong, M.H. & Malumuth, E.M. 2010, WFC3 ISR 2010-05